PHYSICAL REVIEW C

NUCLEAR PHYSICS

THIRD SERIES, VOLUME 33, NUMBER 1 JANUARY 1986

Measurements of elastic neutron scattering from ^{12}C and ^{32}S at 30.3 and 40.3 MeV: Limits on charge symmetry breaking in the nuclear mean field

J. S. Winfield, Sam M. Austin, R. P. DeVito,* U. E. P. Berg,† Ziping Chen, and W. Sterrenburg‡

National Superconducting Cyclotron Laboratory and Department of Physics and Astronomy, Michigan State University, East Lansing, Michigan 48824

(Received 14 June 1985)

Angular distributions have been measured for $^{32}S(n,n)$ and $^{12}C(n,n)$ at $E_n = 30.3$ and 40.3 MeV. Coupled channels analyses of these and lower energy data have been performed and the resulting potentials compared with those from similar analyses of proton scattering. Data for ^{28}Si and ^{40}Ca are also reanalyzed in the same manner. After correcting for purely Coulomb effects, twice the differences between the neutron and proton volume integrals per nucleon of the real potential, $2(J_n - J'_p)$, are as follows: 0 ± 24 (^{12}C), -30 ± 11 (^{28}Si), -29 ± 16 (^{32}S), and 8 ± 14 (^{40}Ca) MeV fm^3. These results are used to put limits on charge symmetry breaking in the nuclear mean field.

I. INTRODUCTION

Whether charge symmetry is broken in the nucleon-nucleon interaction, and if so by how much, has long been a question of interest to nuclear and particle physicists.[1] From theory[2,3] several sources of charge symmetry violation are predicted, the most important ones caused by the mixing of mesons of different isospin (in particular π^0-η and ρ^0-ω mixing), two pion exchange, π^0-γ exchange, radiative corrections of meson-nucleon coupling constants, and by the electromagnetic mass differences of baryons. More fundamentally, the difference in the up and down quark masses has been shown[4] to make the interaction between two neutrons slightly more attractive than that between two protons. Quark-level descriptions of the ^{3}He-^{3}H system have recently been extended[5,6] to show an alternative view of charge symmetry breaking (CSB) at the hadronic level, basically because the mass difference between a six-quark bag formed from two protons and that formed from two neutrons is not equal to twice the proton-neutron mass difference.[7] In fact by using a hybrid quark-nucleon model in which nucleons can form multiquark bags at short distances, the ^{3}He-^{3}H mass difference can be resolved.[5] Koch and Miller[6] suggest that a substantial fraction of the Nolen-Schiffer anomaly (see below) for other mirror nuclei may also be explained in this way. Thus from a variety of standpoints there is a clear prediction that the force between two protons, v_{pp}, is not equal to the force between two neutrons, v_{nn}. In other words, there exists a charge asymmetric interaction which preserves symmetry with respect to the interchange of nucleons in isospin space (the third kind of nucleon-nucleon interaction in the classification of Henley and Miller[2]).

On the experimental front, measurements on the two-body interaction have become more precise; the $^1S_0$ scattering lengths, a_{nn} and a'_{pp} for the two-neutron and (Coulomb-corrected) two-proton systems, are now thought to be equal within 1 to 2 fm and the effective ranges r_{nn} and r_{pp} to be equal within approximately 0.2 fm. Currently the best experimental values, $a'_{pp} = -17.1\pm0.2$ fm (Ref. 8) and $a_{nn} = -18.6\pm0.5$ fm (Ref. 9), indicate a small violation of charge symmetry. However, ambiguities associated with the techniques for removing the purely Coulomb effects from r_{pp} and a_{pp} remain. More sophisticated experiments involving measurements of the analyzing power in np collisions are in progress[10,11] and may be able to put limits on charge asymmetric interactions which are *not* symmetric under the interchange of nucleons in isospin space (class IV interactions,[2] which affect the np system only).

Evidence concerning charge symmetry breaking in the nuclear mean field is far less extensive. Perhaps the most persuasive example is the so-called Nolen-Schiffer or Coulomb-energy anomaly,[12] that the binding energy of mirror nuclei (e.g., ^{41}Ca and ^{41}Sc) differs by 5—10 % more than one would predict based on simple theories taking into account the effects of the Coulomb interaction. This anomaly is of long standing and remains in spite of substantial theoretical effort.[13] Many detailed corrections to the simple theory have been calculated but they are generally small and tend to cancel. Following a survey of the situation, Negele[14] concluded that the simplest explana-

tion was that the single particle potential felt by a valence neutron is more attractive than that felt by a valence proton. The difference required to explain the anomaly, corresponding to a volume integral of about 20 MeV fm^3 (Ref. 15), was consistent with existing limits from the two-nucleon interaction. The anomaly remains perhaps the best evidence for CSB in the nuclear mean field.

Another phenomenon which might exhibit CSB is the difference in scattering of neutrons and protons from an isospin zero ($N=Z$) target such as ^{40}Ca. Given Negele's estimate, and assuming that the difference is of the same magnitude at the positive energies characteristic of scattering, a simple folding model indicates that the real potential felt by a neutron should be about 5% deeper than that felt by a proton. Such differences are comparable to the accuracy obtained in the extraction of real optical model potentials from state-of-the-art proton and neutron scattering data. Noting this fact, DeVito *et al.*[16] compared their neutron scattering data from ^{40}Ca with proton scattering data. After correcting for the purely Coulomb interaction, they found that the proton potential was slightly deeper than the neutron potential; opposite to the direction of the effect assumed by Negele and different from it by about three standard deviations. A check of this result by the comparison of neutron and proton scattering data from other $N=Z$ targets is important, especially now that quark-model estimates may explain the Coulomb energy anomaly and presumably lead to CSB forces in scattering as well.[17] Furthermore, the lower mass targets studied here could yield tighter limits on CSB since the contribution from Coulomb effects will be smaller.

A weakness in the analysis of DeVito *et al.*[16] is their neglect of channel coupling to the 3^- state at 3.74 MeV in ^{40}Ca. It was argued that this neglect was justified since coupling effects should be similar for proton scattering and neutron scattering and would cancel in the difference. A numerical test appeared to validate this assumption. However, one of the more surprising results reported in the present paper is the significantly different effect of coupling to the low-lying collective states for proton and neutron scattering. Some reasons underlying this difference are discussed in the Appendix.

In this paper we first present experimental results for the elastic scattering of 30.3 and 40.3 MeV neutrons from targets of ^{32}S and ^{12}C. These data, together with data at lower energies, are then analyzed in a phenomenological coupled channel optical model and the resulting potentials are compared with those obtained in similar analyses of available proton scattering data. Similar comparisons are carried out for previously published data on ^{40}Ca and ^{28}Si. After correcting for purely Coulomb effects (Sec. III A) and particle-core polarization (Sec. III C), the remaining difference between the proton and neutron real potentials is identified with charge symmetry breaking (CSB).

We regard this as a preliminary investigation to determine whether one can expect to obtain CSB information from present neutron and proton scattering data. We find that reasonably tight limits on CSB can be set, but more refined calculations are necessary to obtain a truly definitive result.

II. EXPERIMENTAL PROCEDURES

The measurements were performed using the Michigan State University (MSU) beam swinger time-of-flight system as modified for neutron scattering.[18] Neutrons produced by the ^{7}Li(p,n)^{7}Be(g.s. + 0.429 MeV) reaction were scattered from a cylindrical target and detected in a liquid scintillation counter with an overall time resolution of about 1.0 ns. This yielded an energy resolution for the elastic peak of better than 1.0 MeV FWHM, sufficient to resolve the first excited states of ^{12}C (4.44 MeV) and ^{32}S (2.23 MeV). Pulse shape discrimination was utilized to eliminate the γ-ray background. The neutron detectors were 7—8 m from the scatterer and situated in a room separated from the swinger vault by a 1.8 m thick concrete wall, except for a hole to transmit the scattered neutrons. Additional shielding against neutrons coming directly from the neutron production target was provided by a movable 1.1 m long iron shadow bar. A monitor time-of-flight detector was mounted rigidly to the beam swinger so as to measure neutron flux from the production reaction at a fixed angle near 22°. This monitor was used to normalize the flux from run to run. Air scattering background was accounted for by measuring target-in and target-out spectra at each angle; a small correction was made to account for the fact that some of those air scattered neutrons originating behind the sample were absorbed by the sample on their way to the detector. Observation of the ^{7}Li(p,n) flux at 0° measured the product of incident neutron flux and detector efficiency and yielded the absolute normalization to within ±3%. Corrections also were made for dead time and neutron source anisotropy.

TABLE I. Experimental parameters.

Target	E_n (MeV)	ΔE_n (MeV)	Target size[a] (cm×cm)	Target mass (g)	Chemical purity[b] (%)
^{12}C	40.3	0.95	3.40×2.64	33.077	>98
^{32}S	30.3	0.8—0.9	2.86×3.17	42.417	99.9
^{32}S	40.3	0.95	2.86×3.17	42.417	99.9

[a]Targets are right circular cylinders of dimensions (height×diameter).

[b]All targets have the naturally occurring isotopic abundance of 98.89% ^{12}C for carbon and 95.0% ^{32}S for sulfur.

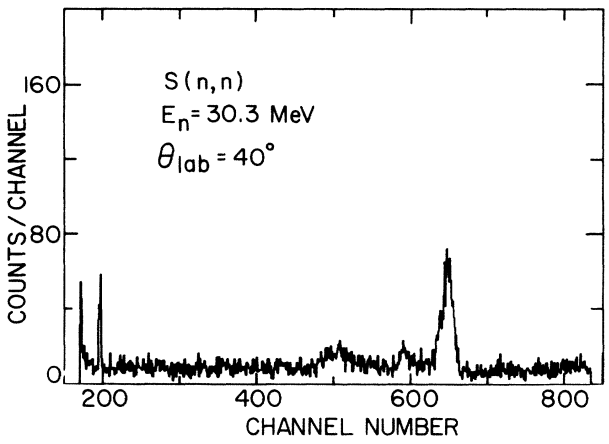

FIG. 1. Time-of-flight spectrum for neutrons scattered from a ^{32}S target before subtraction of air-scattered background. The incident neutron energy was 30.3 MeV, the detection angle was 40° (lab).

The sulfur target was produced by pouring molten sulfur into a Pyrex beaker in layers thin enough so the solidification could be monitored to ensure that no holes were being formed in the target. When the desired amount of material was solidified, the beaker was heated so as to melt the outer surface of the sulfur mass and was then cooled; best results were achieved with fast cooling in a water bath. The glass beaker was then broken away from the sulfur, yielding a target with a hard surface. The target used in the experiment was broken apart after the experiment was complete and no voids were discovered.

Further details of the experimental procedures and analysis may be found in Ref. 18 and Table I. A typical spectrum is shown in Fig. 1 and resulting angular distributions in Figs. 2 and 3.

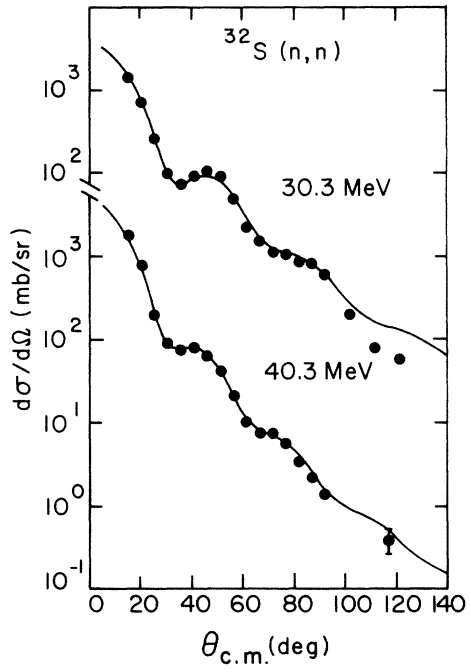

FIG. 2. Center-of-mass cross sections for $^{32}S(n,n)^{32}S$ at 30.3 and 40.3 MeV. Relative uncertainties are typically 4% and are shown when larger than the point. In addition there is a normalization uncertainty of ±3%. The curves are CC fits to the data as discussed in the text.

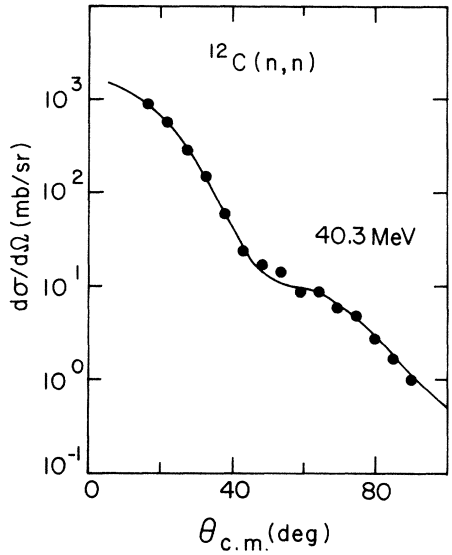

FIG. 3. Center-of-mass cross section for $^{12}C(n,n)^{12}C$ at 40.3 MeV. Relative uncertainties are typically 4% and are shown when larger than the point. In addition there is a normalization uncertainty of ±3%. The curve is a CC fit to the data as discussed in the text.

III. ANALYSIS AND RESULTS

A. General procedure

Our general procedure for estimating the size of any CSB potential follows that of DeVito *et al.*[16] Proton and neutron scattering data are analyzed with an optical model (OM) code for as wide an energy range as practical. For our purposes, the bombarding energy should not be so low that compound nuclear effects are significant and not so high that a linear approximation to the energy dependence of the local potential is no longer valid. The volume integrals per nucleon of the real optical potentials for the protons, J_p/A, are plotted against the incident energy and the best straight-line fit is found (see, e.g., Fig. 4). This linear function is subtracted away from the volume integrals of the real optical potentials found for the neutron scattering data, J_n/A, and the average of these differences, $(J_n-J_p)/A$, is found.

Before this average can be related to possible CSB effects, it is necessary to correct for a trivial consequence of the Coulomb force, namely that the protons are slowed down by Coulomb repulsion. Then, because the (local) optical model potential (OMP) is energy dependent, decreasing with increasing energy, the protons feel a stronger nuclear attraction than neutrons of the same incident energy.[19] To determine this correction for ^{28}Si we follow the procedure described by DeVito *et al.*[16] whereby

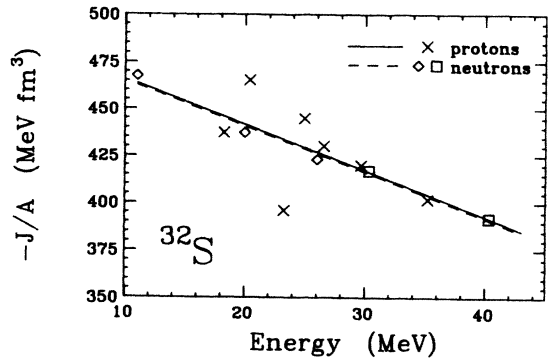

FIG. 4. Volume integrals per nucleon of the real potential for proton and neutron scattering from ^{32}S plotted versus incident energy. The data are from the following sources: squares, present work; diamonds, Ref. 27; crosses, Ref. 29. The lines are least-squares fits. The neutron results were fitted assuming the same slope as obtained for protons.

a series of elastic proton scattering calculations with different energies are compared with a given neutron scattering calculation. The Coulomb shift, ΔE_C, is taken as the difference in energy which results in the diffraction maxima and minima occurring at the same angle. In practice, only two minima and one maximum fall in the range under consideration, $20° < \theta_{\text{c.m.}} < 150°$, and these are often broad and ill-defined. In order to sharpen the peaks and valleys, the calculations were repeated with the spin-orbit potential, V_{so}, turned off and a more consistent set of values was obtained. An average of the results for ^{28}Si gives $\Delta E_C(^{28}\text{Si}) = 5.7 \pm 0.4$ MeV, which is somewhat less than the average Coulomb energy (6.03 MeV) of a proton in the electric field of ^{28}Si. A change in this direction is expected since absorption prevents some projectiles from reaching the center of the nucleus where the Coulomb potential is largest. Combining ΔE_C for ^{28}Si with that obtained earlier for ^{40}Ca, $\Delta E_C(^{40}\text{Ca}) = 7.0 \pm 0.6$ (Ref. 16), and assuming a functional form of $Z/A^{1/3}$ (Ref. 20), yields estimates of $\Delta E_C(^{32}\text{S}) = 6.1 \pm 0.6$ MeV and $\Delta E_C(^{12}\text{C}) = 3.2 \pm 0.4$ MeV.

To relate the differences between real optical potentials to the CSB potential of Negele[14,15] a simple folding model is used. Denoting the volume integrals of the two-body pp, pn, and nn interactions by J^{pp}, J^{pn}, and J^{nn}, we have

$$J'_p = ZJ^{pp} + NJ^{pn} ,$$

$$J_n = ZJ^{pn} + NJ^{nn} ,$$

where J'_p is the volume integral for proton scattering corrected for the Coulomb shift as described above. Defining the CSB interaction as $J^{CSB} = J^{nn} - J^{pp}$ and since here $N = Z = A/2$, we obtain

$$J^{CSB} = 2(J_n - J'_p)/A .$$

Many spherical OM analyses of nucleon scattering from the target nuclei under consideration here have been reported in the literature. For example, both ^{28}Si(p,p) (Ref. 21) and ^{28}Si(n,n) (Ref. 22) have been analyzed using similar geometrical parameters and one might consider using those results here. However, because of the strength of the coupling to the first 2^+ states in some of these nuclei, for example in ^{28}Si $\beta_2 = -0.4$ (Ref. 23), it seemed prudent to analyze the data using the coupled channels (CC) formalism. We anticipated that the individual volume integrals might be affected, but that the change in $(J_n - J_p)$ would be insignificant. The code ECIS (Ref. 24) was used for the CC analyses; these are discussed in more detail in subsection B.

A deformed nucleon potential of the form

$$U = -Vf(r,R_v,a_v) - iW_V f(r,R_w,a_w) + 4a_w iW_D \frac{d}{dr} f(r,R_w,a_w) + \left[\frac{\hbar}{mc}\right]^2 V_{so} \mathbf{l}\cdot\mathbf{s} \frac{1}{r}\frac{d}{dr} f(r,R_{so},a_{so})$$

was used. For simplicity the geometries of the volume and surface absorption terms were kept equal. The form factor f is of a Woods-Saxon type

$$f(r,R_x,a_x) = \{1 + \exp[(r - R_x)/a_x]\}^{-1} ,$$

where $R_x(\Omega)$ is a potential radius dependent on the angle made with the symmetry axis. The nuclei ^{12}C, ^{28}Si, and ^{32}S were assumed to be rigid symmetric rotors with quadrupole deformations. Thus

$$R_x = r_x A^{1/3}[1 + \beta_2 Y_2^0(\Omega)] .$$

In the case of proton scattering, a Coulomb potential $V_C(r_C)$ was included (see below). All the potentials, real, imaginary, spin orbit, and Coulomb were deformed, with the same deformation assumed for each.

The starting parameters for the Woods-Saxon OM potentials in the searches were taken from the literature. In general, the geometrical parameters of the real and imaginary wells were kept fixed during the searches and were assumed to be the same for neutron and proton scattering. Only the well depths were allowed to vary. It seems reasonable to use fixed geometries considering the relatively small energy range covered (15 to 40 MeV in general), but, because of core polarization effects, it is not so clear that the geometries used in the analysis of neutron and proton scattering should be the same. In subsection C we make an estimate of the (small) change expected in our results due to the difference in proton and neutron distributions.

In all calculations, the spin-orbit potential (assumed to be real) was set to values, or averages of values, reported in the literature for cases where polarization data were included in the input data to a search code. The central potential parameters are rather insensitive to the spin-orbit potential.

The Coulomb potential was taken to be that of a uniform charge distribution with a radius

$$R_C = r_C A^{1/3}[1 + \beta_L Y_L^0(\Omega)] .$$

The values of r_C found in various OM parameter sets in the literature (typically $r_C = 1.2$ fm) are clearly arbitrary to some degree; normally one is insensitive to effects of the magnitude involved here ($\sim 1\%$ in V). We therefore

have used instead values of r_C related to the experimentally measured rms charge radius, R_{ch}, of the target nucleus. These values were obtained from Ref. 25, where the relationship $R_{ch}=\langle r^2\rangle^{1/2}=\sqrt{3/5}R_C$, is assumed; they are noted in the respective tables of results. The consequence of the use of those values rather than $r_C=1.2$ fm, say, is J^{CSB} values typically 8 MeV fm^3 more negative.

Since we are concerned with deformed potentials, the definition of the volume integral per nucleon used here is

$$J/A=\int U(r,\Omega)dr/A\ .$$

These integrals were evaluated numerically.

In regard to the estimation of uncertainties in our analyses, we have *not* used the error estimates on the optimized values of the potential depths which are given by the search code (ECIS); instead, equal weight has been given to each energy point during the fits to the proton and neutron results and uncertainties on J^{CSB} have been evaluated from the standard deviation of the points around these fits. The reasons for choosing not to use the uncertainty estimates from the search code were the following: (i) to avoid biasing because of possible different error estimates on angular distributions taken from different sources, and (ii) to avoid undue weighting on searches which gave a poor fit (viz., large χ^2 per degree of freedom) but an apparently well-determined parameter (presumably indicating that the χ^2 surface was steep for small changes of that parameter in the search). The error estimates from the search code, although not used, are listed in terms of errors on J_V/A in Tables II–VI for comparison purposes.

B. Specific calculations

We now discuss the calculations for each target in more detail.

1. ^{32}S analysis

In addition to analyzing the new data for ^{32}S(n,n) at 30.3 and 40.3 MeV, we have essentially repeated the CC analysis by Tailor[26] of lower energy ^{32}S(n,n) data from Ref. 27 and ^{32}S(p,p) data from De Leo *et al.*,[28,29] but with the Coulomb radius parameter taken as $r_C=1.327$ fm instead of 1.25 fm. Apart from this, the same geometrical parameters as in Refs. 26 and 29 were used and only the parameters V and W_D were searched upon. The volume imaginary well depth W_V was fixed according to the form given in Ref. 29 (see Table II). As did Tailor, we assumed a simple rotational model for ^{32}S, coupling only the ground state and 2^+ first excited state at 2.23 MeV. Although in a more extensive coupling scheme, ^{32}S is better described by a vibrational model, detailed analyses[26,30] show no significant difference in the ground state potential between the two models. A quadrupole deformation parameter of $+0.283$ (Ref. 29) was assumed throughout. The results of the searches are given in Table II.

Following the procedure outlined in subsection A, a straight line was fitted to the ^{32}S(p,p) real volume integrals using an unweighted least squares procedure (Fig. 4). This yielded

$$-J_p/A=490.2-2.45E_p\ \text{MeV fm}^3$$

or, correcting for the Coulomb shift (6.1 MeV) discussed above,

$$-J'_p/A=475.2-2.45E_p\ \text{MeV fm}^3\ .$$

The fit with the same slope to the neutron results (which is equivalent to finding the average deviation of J_n/A from the fitted proton line) yields

$$-J_n/A=489.8-2.45E_n\ \text{MeV fm}^3\ .$$

Then, following the definition in subsection A, we find

$$J^{CSB}=2(J_n-J'_p)/A=-29\pm16\ \text{MeV fm}^3\ ,$$

where the uncertainty comprises contributions from the fits to the (p,p) and (n,n) volume integrals and from ΔE_C. The procedure is presented graphically for all targets in Fig. 5.

TABLE II. Results of the CC analysis for ^{32}S. The geometrical OM parameters were the following: $r_v=1.158$, $a_v=0.703$, $r_w=1.215$, $a_w=0.640$, $r_{so}=1.03$, $a_{so}=0.66$, and $r_C=1.327$ (all in fm); in addition, $W_V=0.0$ for $E<19$ MeV, $W_V=0.4E-7.96$ MeV for $E>19$ MeV, and $V_{so}=6.1$ MeV.

E (MeV)	V (MeV)	W_D (MeV)	χ^2/N	$-J_V/A$ (MeV fm^3)	$-J_W/A$ (MeV fm^3)
(a) Proton scattering					
18.24	48.69	5.13	19.8	437.3± 5.6	84.2
20.37	51.81	6.89	21.7	465.3± 5.0	114.9
23.24	44.08	4.96	48.4	395.8±11.3	94.3
24.95	49.53	6.80	59.8	444.8±11.3	131.2
26.55	47.91	5.47	23.7	430.2± 5.9	115.6
29.64	46.75	4.11	20.7	419.8± 9.5	104.3
35.20	44.73	2.83	28.5	401.7± 9.8	105.8
(b) Neutron scattering					
30.3	46.43	4.35	8.4	416.9± 5.4	111.7
40.3	43.63	2.64	6.5	391.8±10.4	122.5

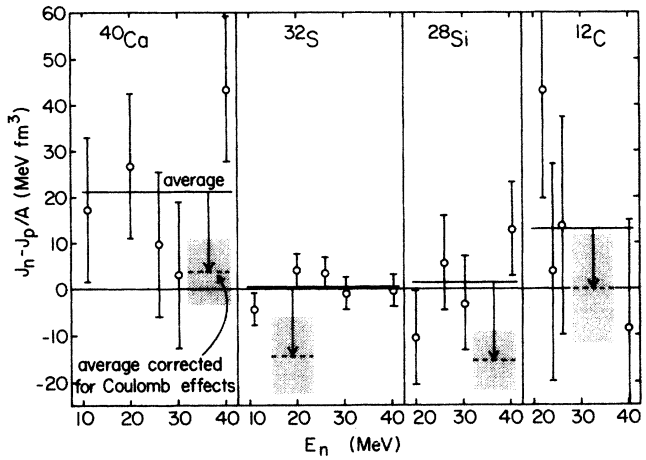

FIG. 5. Differences of the real volume integrals per nucleon for proton and neutron scattering from ^{40}Ca, ^{32}S, ^{28}Si, and ^{12}C. The points are the differences between the fitted line for protons (Figs. 4, 6, 7, and 9) and the measured values for neutrons. The solid lines are the averages of these differences in each case, the error bars on the points show the standard deviation about this mean. The dashed lines within the shaded regions are the averages with their associated uncertainties after correcting for Coulomb effects.

2. *Analysis of ^{12}C*

Proton scattering data from Refs. 31 and 33 and neutron scattering data from Ref. 32 together with the data presented here for 40.3 MeV have been analyzed assuming a similar rotational model as for ^{32}S, with only the ground and 2^+ (4.44 MeV) states included. A quadrupole deformation parameter of -0.6 was used throughout (De Leo *et al.*[33] suggest that the 4^+ state at 14.08 MeV in ^{12}C is primarily populated by two-step processes and that if β_4 is set to 0.0, β_2 should be approximately -0.6). The geometry of the optical potentials was taken from Ref. 33 and, as done in that work, W_V was set to zero. If W_V was allowed to vary during the searches, its behavior was erratic with negative values for a few low energy points.

The resulting volume integrals are tabulated in Table III and plotted in Fig. 6. A linear fit to the proton results yields

$$-J_p/A = 583.1 - 4.09E_p \text{ MeV fm}^3 ,$$

or, correcting for the Coulomb shift,

$$-J'_p/A = 570.0 - 4.09E_p \text{ MeV fm}^3 .$$

The lower energy ^{12}C(n,n) points (20.8 and 22 MeV) display anomalously small values of J_n/A. The reduced χ^2 of the fit to the experimental angular distribution at 20.8 MeV is unusually large [more than twice those for the other (n,n) values]. There is therefore good reason to disregard this point. We then obtain

$$-J_n/A = 570.0 - 4.09E_n \text{ MeV fm}^3$$

which leads to

$$J^{CBS} = 0 \pm 24 \text{ MeV fm}^3 .$$

This is the situation shown in Fig. 5 and discussed hereafter.

TABLE III. Results of the CC analysis for ^{12}C. The geometrical OM parameters were the following: $r_v = 1.064$, $a_v = 0.623$, $r_w = 1.20$, $a_w = 0.60$, $r_{so} = 1.0$, $a_{so} = 0.6$, $r_C = 1.394$ (all values in fm). In addition, $V_{so} = 6.0$ MeV. W_V was held fixed at 0.0 MeV during the searches.

E (MeV)	V (MeV)	W_D (MeV)	χ^2/N	$-J_V/A$ (MeV fm^3)	$-J_W/A$ (MeV fm^3)
(a) Proton scattering					
15.9	58.79	3.22	98.0	513.4±17.6	72.4
17.4	56.65	3.81	154.9	494.8±24.5	85.6
18.5	56.16	3.99	114.9	490.4±25.7	89.6
20.0	59.66	3.81	48.1	521.1±33.2	85.5
22.7	57.51	3.83	47.1	502.3±21.2	86.1
24.7	54.30	5.96	80.2	474.3±28.4	134.0
27.3	57.98	4.82	30.5	506.4±18.3	108.4
28.9	52.78	4.20	22.7	461.0±16.3	94.3
29.9	53.53	5.12	15.4	467.5±13.2	115.1
30.0	52.21	5.24	27.0	456.0±10.9	117.7
33.2	52.32	5.11	21.9	456.9±15.9	114.8
35.2	51.32	4.66	13.1	448.2±10.1	104.8
35.2	47.16	3.64	12.1	411.8± 8.9	81.7
39.9	47.13	4.23	23.8	411.6±14.4	95.1
(b) Neutron scattering					
20.8	49.36	5.11	18.0	431.1±17.8	114.9
22.0	51.51	4.79	8.9	449.9± 8.9	107.7
24.0	55.09	4.07	6.7	481.2± 7.9	91.5
26.0	53.02	4.75	3.4	463.1± 7.0	106.8
40.3	48.88	6.71	8.3	426.9±11.6	150.6

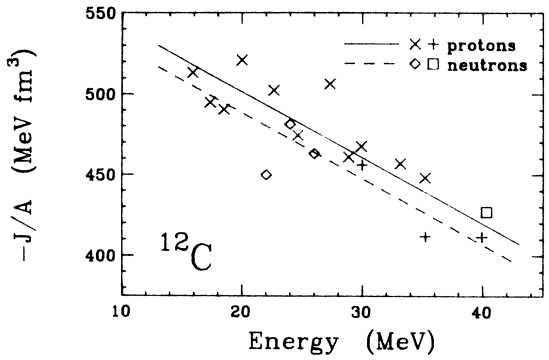

FIG. 6. Volume integrals per nucleon of the real potential for proton and neutron scattering from ^{12}C plotted versus incident energy. The data are from the following sources: square, present work; diamonds, Ref. 32; diagonal crosses, Ref. 31; vertical crosses, Ref. 33.

3. *^{28}Si analysis*

For the ^{28}Si target the geometrical parameters of the OMP were taken from De Leo *et al.*[21] In most cases, only the 0^+ ground and 2^+ (1.78 MeV) states in ^{28}Si were coupled, a fixed coupling constant, $\beta_2=-0.4$ (Ref. 23) was used, and only elastic scattering data were searched on. As a check, several cases were run for both (p,p) and (n,n) with coupling to the 4^+ (4.62 MeV) state included (β_4 was fixed at $+0.15$, β_2 free to vary) and data for the 2^+ excitation used as additional input to the search. The results of this check are listed in Table IV. Generally, the results for 0^+-2^+-4^+ coupling differ by less than the uncertainties on the points from the basic 0^+-2^+ searches, showing that the quadrupole deformation and the elastic scattering data dominate the calculation.

The real and imaginary potential depths obtained in the 0^+-2^+ searches are listed in Table V. From fits to the proton real volume integrals, we find

$$-J_p/A = 503.5 - 2.92E_p \text{ MeV fm}^3$$

or, correcting for the Coulomb shift (5.7 MeV) discussed in subsection A,

$$-J'_p/A = 486.9 - 2.92E_p \text{ MeV fm}^3 .$$

The fit with the same slope to the neutron results gives

$$-J_n/A = 501.9 - 2.92E_n \text{ MeV fm}^3$$

which gives

$$J^{CSB} = -30 \pm 11 \text{ MeV fm}^3$$

(see Figs. 5 and 7).

Because the data are somewhat more extensive than for the other deformed nuclei studied here, we have chosen this case for an examination of differences induced by channel coupling. To this end searched potential depths from spherical analyses of ^{28}Si(p,p) data by De Leo *et al.*[21] and ^{28}Si(n,n) data by DeVito *et al.*[22] are compared with equivalent CC analyses in Fig. 8 (note that separate CC calculations were performed with $r_C=1.2$ fm in order to make a fair comparison with the spherical values). It is seen that the introduction of coupling decreases the magnitude of the real potential depth for proton scattering but the opposite effect occurs for neutron scattering. This has been shown not to be an effect owing to the different weighting of data points in the (p,p) and (n,n) angular distributions by restricting the range of the proton data to $<100°$ where the relative errors are all similar for both cases. The difference in behavior of the proton and neutron OMP's when coupling is turned on is clearly important with respect to the deduced value of $(J_n - J'_p)/A$ and hence J^{CSB}. Indeed, the result for the spherical OM analyses is $J^{CSB} = -1 \pm 9$ MeV fm^3. This point will be discussed further in the Appendix.

4. *^{40}Ca reanalysis*

In view of the ^{28}Si result—in particular, the substantial shift to more negative values of J^{CSB} when channel coupling is introduced—a new analysis of the ^{40}Ca data within the CC model was clearly called for. Accordingly, we have used the procedure outlined above for coupling between the 0^+ ground and 3^-, 3.74 MeV states in ^{40}Ca. A vibrational model with a one-phonon (octupole) excitation to the 3^- state and coupling strength $\beta_3=0.24$ (Ref. 34) was taken to describe the scattering. Three ^{40}Ca(p,p) and five ^{40}Ca(n,n) angular distributions quoted in Ref. 16 were reanalyzed. The same OM geometrical parameters as in that analysis were used, with the usual exception of r_C for which the value of 1.314 fm (Ref. 25) was used rather than 1.2 fm. The results are given in Table VI and Fig. 9.

TABLE IV. Comparison of ^{28}Si results with 0^+-2^+ coupling to test calculations with 0^+-2^+-4^+ coupling. OM geometries as in Table V except $r_C=1.2$ fm.

Calculation	$-J/A$ (0^+2^+)[a] (MeV fm^3)	β_2[b]	$-J/A$ $(0^+2^+4^+)$[b] (MeV fm^3)	Difference (MeV fm^3)
20 MeV (n,n)	455.3±7.7	−0.41	460.2± 7.2	4.9±10.5
26 MeV (n,n)	421.6±5.0	−0.40	425.5±10.5	3.9±11.6
20 MeV (p,p)	442.4±3.7	−0.34	439.5± 5.5	−3.0± 6.6
37 MeV (p,p)	393.3±5.8	−0.35	400.3± 2.3	7.0± 6.2

[a]Results of normal procedure with only the 2^+ state coupled to the ground state and a fixed $\beta_2=-0.4$.
[b]Results of test calculations with 2^+ and 4^+ states coupled to the ground state, β_2 free to vary, and a fixed $\beta_4=+0.15$.

TABLE V. Results of the CC analysis for ^{28}Si. For all searches the geometrical parameters were kept constant at $r_v=1.17$, $a_v=0.673$, $r_w=1.33$, $a_w=0.575$, $r_{so}=1.07$, $a_{so}=0.78$, $r_C=1.328$ (all in fm).

E (MeV)	V (MeV)	W_V (MeV)	W_D (MeV)	V_{so} (MeV)	χ^2/N	$-J_V/A$ (MeV fm^3)	$-J_W/A$ (MeV fm^3)
(a) Proton scattering							
18.2	48.92	2.38	3.55	8.77	18.2	456.7± 4.6	93.5
20.2	46.92	0.94	4.29	5.41	17.3	438.1± 3.6	89.4
22.7	47.60	1.74	3.64	6.01	35.5	444.4± 6.2	87.4
25.4	46.64	1.54	3.75	8.49	22.5	435.4± 7.5	86.9
29.5	43.77	3.35	2.41	7.00	42.3	408.7±12.1	84.7
30.5	42.80	3.01	2.36	6.49	32.2	399.6±10.8	79.6
31.5	43.78	3.27	2.38	5.96	18.0	408.7± 8.0	83.1
34.7	43.89	6.01	0.79	5.58	5.7	409.8± 4.8	87.6
37.2	41.85	6.03	0.60	5.42	6.7	390.7± 5.7	84.4
40.2	42.31	6.38	0.60	4.88	9.1	395.0± 6.6	88.7
(b) Neutron scattering							
20.0	48.76	6.63	1.12	6.00	1.75	455.3±7.7	101.2
26.0	45.15	5.55	3.35	6.00	2.50	421.6±5.0	128.6
30.3	44.74	8.60	1.37	6.00	5.15	417.8±8.2	129.8
40.0	39.98	7.41	1.29	6.00	4.19	373.3±7.0	113.8

TABLE VI. Results of the CC analysis for ^{40}Ca. The geometrical parameters were the following: $r_v=1.152$, $a_v=0.692$, $r_w=1.309$, $a_w=0.549$, $r_{so}=1.01$ fm, $a_{so}=0.75$, $r_C=1.314$ (all in fm); in addition $V_{so}=6.2$ MeV.

E (MeV)	V (MeV)	W_V (MeV)	W_D (MeV)	χ^2/N	$-J_V/A$ (MeV fm^3)	$-J_W/A$ (MeV fm^3)
(a) Proton scattering						
30.3	49.37	0.65	6.69	74.8	416.8±4.1	104.6
40.0	45.36	−2.08	9.06	20.8	383.0±9.4	109.3
61.4	40.48	0.27	7.31	14.5	341.7±8.5	109.5
(b) Neutron scattering						
11.0	52.10	0.55	5.52	13.5	440.0± 3.0	86.5
20.0	48.51	0.91	6.66	7.5	409.5±11.5	107.0
26.0	48.86	0.61	7.66	5.0	412.5± 5.4	118.3
30.3	48.47	−1.63	9.32	11.3	409.2± 8.5	118.0
40.3	40.91	2.66	4.41	9.5	345.4± 8.1	93.3

A linear fit to the proton results gives

$$-J_p/A = 483.0 - 2.34E_p \text{ MeV fm}^3$$

or, correcting for the Coulomb shift,

$$-J'_p/A = 466.7 - 2.34E_p \text{ MeV fm}^3 .$$

The fit with the same slope to the neutron results gives

$$-J_n/A = 462.9 - 2.34E_n \text{ MeV fm}^3 .$$

TABLE VII. Volume integrals of Hartree-Fock potentials (in MeV fm^3) calculated with a Skyrme interaction from Ref. 39.

Core	J_p/A	J_n/A
^{12}C	525.9	528.4
^{28}Si	475.3	479.1
^{32}S	479.0	483.6
^{40}Ca	476.7	481.3

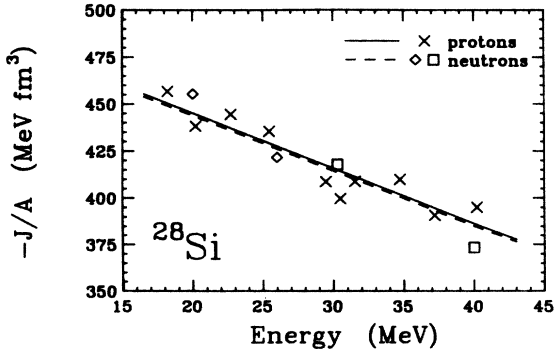

FIG. 7. Volume integrals per nucleon of the real potential for proton and neutron scattering from ^{28}Si plotted versus incident energy. The data are from the following sources: squares, Ref. 22; diamonds, Ref. 27; crosses, Ref. 21.

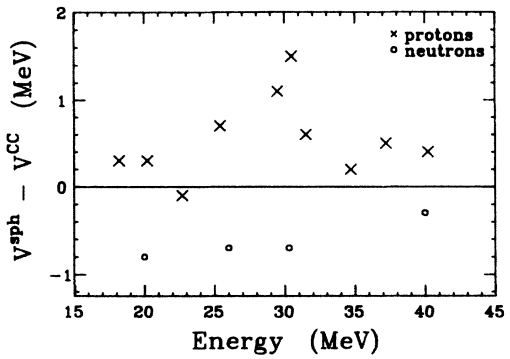

FIG. 8. Comparison of real potential depths obtained from searching ^{28}Si(p,p) and ^{28}Si(n,n) data with spherical and CC codes. The OM geometry was that of De Leo *et al.* (Ref. 21) (with $r_C = 1.2$ fm). In the CC analysis, $\beta_2 = -0.4$. The spherical results for protons have been taken from Ref. 21, and those for neutrons from Ref. 22.

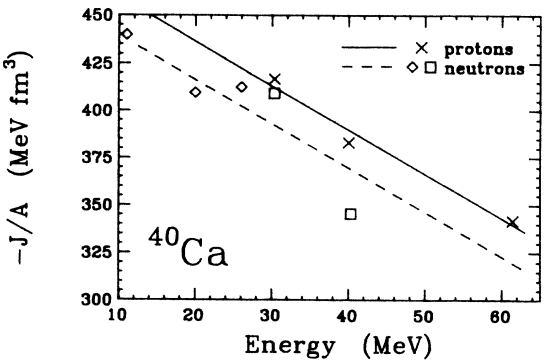

FIG. 9. Volume integrals per nucleon of the real potential for proton and neutron scattering from ^{40}Ca plotted versus incident energy. The data are from the following sources: squares, Ref. 16; diamonds, Ref. 27; crosses, Ref. 35.

Then the value of J^{CSB} from the present analysis is 7.6 ± 14.4 MeV fm^3, to be compared with the spherical result[16] of 14 ± 10 MeV fm^3.

C. Correction for core polarization

There is an effect due to the mutual Coulomb repulsion of protons in a nucleus which may give rise to a measurable difference between proton and neutron scattering even if no charge symmetry breaking is present in the nucleon-nucleon force. The difference between the proton and neutron distributions is significant, with protons pushed to larger radii[36] [in the context of bound nuclei, this is known as the Auerbach, Kahana, Weneser[37] (AKW) effect]. Since neutron projectiles interact mostly with protons in the target and vice versa ($V_{pn} \approx 4V_{pp}$), and absorption limits the likelihood of the projectiles being found in the central region where neutron densities are higher, core-polarization effects enhance J_n relative to J_p.

In Table VII we compare the volume integrals of Hartree-Fock potentials for *bound* protons and neutrons calculated[38] with a charge-symmetric Skyrme interaction (SGII) of van Giai and Sagawa.[39] It is seen that $|J_p/A| < |J_n/A|$ for all targets, as expected. This would give an apparent charge symmetry breaking potential of negative sign. From the differences in these volume integrals, one can obtain rough estimates of the correction to J^{CSB} for core-polarization effects (Table VIII). The uncertainty on these estimates has been taken to be the maximum deviation when either Skyrme interactions SIII or SVI from Beiner *et al.*[40] are used instead. It is not clear, however, how the core polarization correction for nucleons in the scattering states should be compared with these values—this uncertainty may therefore be underestimated.

IV. DISCUSSION AND CONCLUSIONS

The final values of J^{CSB} are listed in Table VIII. The results for the four targets are only marginally consistent: the mean (-9 ± 7 MeV fm^3) has a χ^2 of 5.5 which corresponds to a confidence level of 13%. It seems likely either that the quoted uncertainties are underestimated or that some target-dependent effect has been omitted. One test of the uncertainty estimates on the fitted parameters is to repeat searches with somewhat different OM geometries. This was done for the ^{28}Si data; the geometrical parameters for the real and imaginary wells from Fabrici *et al.*[41] were used:

$$r_v = 1.148 \text{ fm}, \quad a_v = 0.663 \text{ fm},$$

$$r_w = 1.330 \text{ fm}, \quad a_w = 0.600 \text{ fm},$$

TABLE VIII. Adjustments to J^{CSB} and final values (all in MeV fm^3).

Target	Uncorrected value	Core polarization[a]	Final J^{CSB}
^{32}S	-29 ± 16	$+9.2 \pm 0.9$	-20 ± 17
^{12}C	0 ± 24	$+5.1 \pm 0.4$	5 ± 24[b]
^{28}Si	-30 ± 11	$+7.5 \pm 0.8$	-23 ± 11
^{40}Ca	8 ± 14	$+9.1 \pm 0.5$	17 ± 14

[a]Estimate of change in J^{CSB} when core polarization is taken into account (see the text).

[b]From the fit to neutron data with $E_n > 21$ MeV. If the 20.8 MeV data are included, we obtain a final J^{CSB} of 22 ± 29 MeV fm^3.

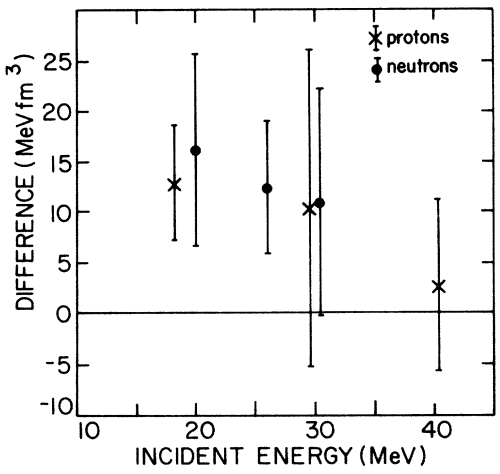

FIG. 10. A comparison of volume integrals of the real potential for nucleon scattering from ^{28}Si analyzed using two different sets of geometrical OM parameters. The values plotted are the difference between the volume integrals calculated using the geometry of Ref. 41 and those calculated using the geometry of Ref. 21 for various incident energies and projectile types. The error bars correspond to the uncertainty on the searched potential as given by the computer code.

with the same spin-orbit and Coulomb potential parameters as before. The differences in the volume integrals resulting from searches with this geometry and those previously obtained are shown in Fig. 10. There is a systematic dependence of the individual volume integrals on the particular choice of geometry chosen, but the differences for proton and neutron scattering are equal within errors (mean values of 9.8 ± 4.5 and 13.2 ± 4.9 MeV fm^3, respectively). It is less simple to evaluate possible target dependent effects.

The ^{12}C result is probably the least reliable of the four. We have noted earlier that the lower energy ^{12}C(n,n) potentials were less deep than those for 24 and 26 MeV (Table III). In addition, one observes some marked fluctuations in the ^{12}C(p,p) points between 20 and 27 MeV. Gaillard *et al.*[42] and Lowe and Watson[43] have shown that resonance phenomena in the p+^{12}C compound system influence this energy region. However, we note that the present results are not altered significantly if the fit to the proton data is restricted to those points above 27 MeV. In general, the fits to the ^{12}C angular distributions are markedly worse than those for the other targets—the large deformation ($\beta_2=-0.6$) may have made the calculations inaccurate, or perhaps other states should have been coupled in explicitly. On the other hand, one might argue that there are too few nucleons in ^{12}C for such an "average" concept as the optical potential to work well at the required level of accuracy.

Although the only type of data used to determine the optical potentials has been differential elastic scattering, test calculations with inelastic data included have not shown any significant differences. In addition, we have compared the potentials with total neutron cross sections and reaction cross sections from the compilations of Refs. 32, 44, and 45. The difference for ^{32}S and ^{28}Si is less than 4%, which is acceptable. For ^{12}C and ^{40}Ca the difference is about 8%, which may indicate some deficiency in the optical model geometry in these cases.

In any case, the initial hope that the study of nuclei lighter than ^{40}Ca might provide tighter limits on charge symmetry breaking has not yet been fulfilled. The Coulomb shift for ^{28}Si contributes less to the uncertainty than that for ^{40}Ca, but the effect of coupling to strongly excited states in the deformed *sd*-shell nuclei is a major complication. The difference between proton and neutron scattering in the behavior of the real potential depth when coupling is introduced was unexpected. The relationship between coupling and the real potential depth is by no means straightforward and the observations made here are not fully understood (see the Appendix). Nevertheless, it seems a fact for nucleon scattering from ^{28}Si that when coupling is introduced, $|J_n/A|$ exceeds $|J'_p/A|$, whereas the two are equal within uncertainties when a spherical OM analysis is made.

If one assumes, as is usually done, that the CSB is negligible, then these measurements yield an estimate of the so-called Coulomb correction. This correction, denoted ΔU_C, is defined by $\Delta U_C = U_p(E) - U_n(E)$ where U_p and U_n are the optical model potentials describing proton and neutron scattering from the same nucleus at an energy E. Previous measurements of these quantities for ^{16}O, ^{28}Si, ^{32}S, and ^{40}Ca are available from spherical OM analyses.[46,22,27] One of the consequences of the present results is that the values of ΔU_C deduced from the CC analyses for ^{32}S and ^{28}Si are much smaller than those values obtained in the spherical OM analyses. This is partly due to our use of more realistic values of the Coulomb radius parameter, but the effect of coupling to the first excited states is the major difference.

It appears that analyses in terms of standard phenomenological OMP's are subject to systematic uncertainties too large to permit an accurate determination of charge symmetry breaking effects in the mean field. Possible improvements might include the use of a folding model to determine the geometry of the real potential (the Woods-Saxon shape is not expected to be accurate for these light nuclei) or the use of model-independent analyses as is done for electron scattering. It is clear that effects of core polarization for unbound nucleons must be included in some fashion, since we have found that its effects for bound nucleons are comparable to any CSB effects. One might also need to consider the effects of coupling to the deuteron channel: the effects of the (p,d,p) reaction on J_V have been shown not to be negligible.[47]

Whether CSB in the nuclear mean field is a viable explanation of the Coulomb energy anomaly remains an open question. Our analysis for ^{40}Ca, including coupled channels effects, still yields a CSB potential inconsistent with this explanation at the two to three standard deviation level. As ^{40}Ca is the heaviest target studied and is subject to the smallest channel coupling effects, the ^{40}Ca result is perhaps the most reliable reported here. On the other hand, the results for the other targets certainly reduce one's confidence in the ^{40}Ca value. Indeed the mean for the three more reliable cases (^{40}Ca, ^{32}S, and ^{28}Si), including the rough correction for core polarization, is

-11 ± 8 MeV fm^3, which is consistent with the value of J^{CSB} proposed by Negele (-19 MeV fm^3) to account for the Coulomb energy anomaly.

Despite the marginal consistency between the results for different targets, it does seem possible to use them to place limits on the magnitude of any CSB term in the mean field. We place a "tight" limit (exclusive of uncertainties on each point) of

$$-23 \text{ MeV fm}^3 \leq J^{CSB} \leq 17 \text{ MeV fm}^3 ,$$

and a "loose" limit (inclusive of the one standard deviation uncertainties) of

$$-36 \text{ MeV fm}^3 \leq J^{CSB} \leq 31 \text{ MeV fm}^3 .$$

ACKNOWLEDGMENTS

The authors wish to thank G. A. Miller for comments and for the results of an unpublished calculation. We also acknowledge helpful discussions with B. A. Brown, G. Bertsch, H. Feshbach, and W. Friedman. This paper is based on research supported in part by the National Science Foundation under Grant No. PHY83-12245.

APPENDIX

In the course of the ^{28}Si analysis we found that the real OM potential depths in proton and neutron scattering were affected in opposite ways when the effects of strongly coupled excited states were included (see Fig. 8). One observes that the introduction of coupling makes the proton potentials somewhat shallower whereas the neutron potentials are deepened. This has a substantial effect on J^{CSB} (which is given by *twice* the difference between the neutron and proton scattering volume integrals) as noted in Sec. III B.

While it is clear that the imaginary OM potential ought to be reduced when coupling to an inelastic channel is explicitly introduced, the effect on the real potential is less obvious. Perey[20] investigated this effect in a computational experiment where the output from a CC calculation was fed into a spherical OM search code and the depths of the real and imaginary potentials, V^{sph} and W^{sph}, were adjusted until the smallest value of χ^2 was obtained. His result for proton scattering on ^{56}Fe was that V^{sph} and W^{sph} both increased in proportion to β^2. The dependence on β^2 is understandable if one regards the spherical OM as representing in some approximate way all terms in the CC expansion:

$$U^{sph} \approx U_{11} + U_{12}G_2U_{21} + \cdots , \quad (1)$$

where U_{11} is the potential for the elastic channel, $U_{\mu\nu}$ is a potential for scattering from channel μ into channel ν, and G_2 is the appropriate Green's function (which includes Coulomb excitation). Both U_{12} and U_{21} are proportional to the coupling strength, hence the dependence of the effective U^{sph} on β^2.

We have carried out computational experiments similar to Perey's but for both protons *and* neutrons scattered from ^{28}Si and ^{32}S. We have also repeated the proton scattering with the Coulomb coupling turned off. The potential parameters for these tests were the same as listed in Table V except that only a surface term was used in the imaginary potential. The results for ^{32}S are shown in Fig. 11 (those for ^{28}Si showed the same trends but were slightly more scattered). An approximately linear dependence on β^2 (except for large β) is indeed observed, but the real potentials for proton and neutron scattering display opposite behavior. A direct comparison of this result to the effect observed in searches with actual data (Fig. 8) is not strictly possible. If one takes the actual data to be "really" CC in nature, Fig. 8 shows the results of spherical and CC searches on CC input, whereas the computational tests (Fig. 11) are for spherical searches on input that ranges from spherical to CC. Nevertheless, it is clear that there is a rather curious difference in the way that real potential depths change when channel coupling is introduced, and we have shown that this is not caused by possible differences in the experimental data. It is also seen from Fig. 11 that Coulomb excitation is responsible for a significant part of the difference, but not all of it.

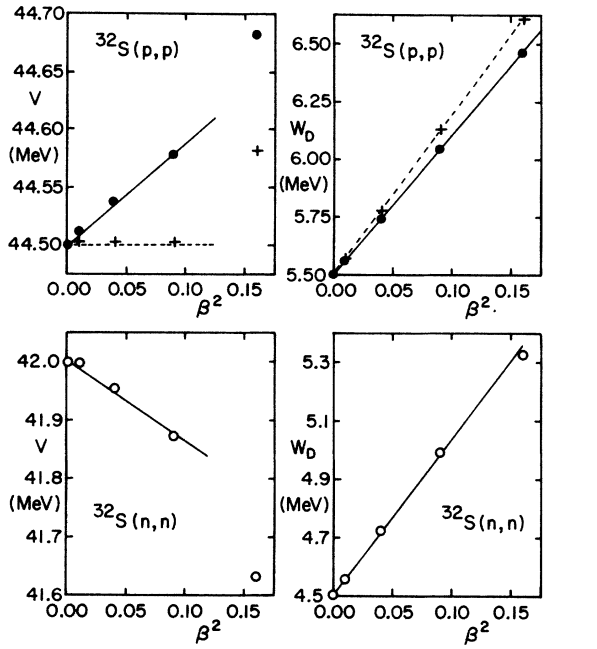

FIG. 11. Equivalent spherical OM well depths fitted to CC calculations as a function of the square of the coupling strength for nucleon scattering from ^{32}S. The (p,p) calculations are for 23 MeV, the (n,n) calculations are for 30 MeV. The crosses are the results without Coulomb excitation. The lines are to guide the eye.

To investigate the cause behind the above observations, we have compared the CC angular distributions for ^{32}S(p,p) and ^{32}S(n,n) as the coupling is increased in strength (Fig. 12). Perey[20] observes that for ^{56}Fe(p,p) the higher diffraction minima move toward smaller angles; it is therefore of interest to see whether the diffraction minima for neutrons scattering move toward larger angles. In order to enhance the diffraction pattern it was necessary to increase the imaginary well depth to 9.5 MeV (Perey used 11 MeV). With this modification it is possible to see

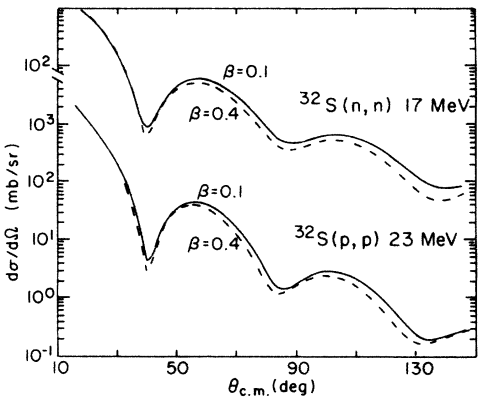

FIG. 12. A comparison of the effect of the coupling parameter β on the calculated elastic angular distribution for proton and neutron scattering on ^{32}S.

a similar shift of the diffraction minima as Perey observed for ^{32}S(p,p) and (but perhaps to a lesser extent) for ^{32}S(n,n). Thus there does not seem to be a clear difference in the qualitative behavior of the (p,p) and (n,n) angular distributions as the effects of coupling to excited states are increased. This seems to imply that the difference observed in the searched potential depths for proton and neutron scattering lies in the way the spherical OM potential has to simulate the effects of coupling, rather than those effects themselves. To investigate this, one might consider the real part of Eq. (1):

$$V^{\rm sph} = {\rm Re}[U^{\rm sph}]$$

$$\approx {\rm Re}[U_{11}] + {\rm Re}[U_{12}G_2U_{21}] + \cdots ,$$

but the Green's function G_2 and the scattering potentials U_{12} and U_{21} are complex quantities, and it is not possible to disentangle the various contributions with the present, simple approach.

In summary, searches with a spherical OM code on calculated CC angular distributions have revealed differences between proton and neutron scattering which are similar to the differences observed when searching on actual data. Thus one can probably rule out possible variations in the quality of (p,p) and (n,n) data as a cause. Coulomb excitation has been shown to account for a significant part of the difference; the reason for the remaining part is not clear at present.

*Present address: Siemens Gammasonics Inc., Des Plaines, IL 60018.

†Present address: Institut für Kernphysik, Justus Liebig Universität, 6300 Giessen, Federal Republic of Germany.

‡Present address: Universitas Gadjah Mada, Yogyakarta, Indonesia..

[1]For a review see, e.g., W. T. H. van Oers, Comments Nucl. Part. Phys. **10**, 251 (1982).

[2]E. M. Henley and G. A. Miller, in *Mesons in Nuclei,* edited by M. Rho and D. H. Wilkinson (North-Holland, Amsterdam, 1979), Vol. I.

[3]S. A. Coon and M. D. Scadron, Phys. Rev. C **26**, 2402 (1982).

[4]P. Langacker and D. A. Sparrow, Phys. Rev. Lett. **43**, 1559 (1979); A. W. Thomas, P. Bickerstaff, and A. Gersten, Phys. Rev. D **24**, 2539 (1981).

[5]J. M. Greben and A. W. Thomas, Phys. Rev. C **30**, 1021 (1984).

[6]V. Koch and G. A. Miller, Phys. Rev. C **31**, 602 (1985); **32**, 1106(E) (1985).

[7]A. W. Thomas, Adv. Nucl. Phys. **13**, 1 (1983).

[8]E. M. Henley, in *Proceedings of the International Conference on Few Particle Problems in Nuclear Interaction, Los Angeles, 1972,* edited by I. Slaus *et al.* (North-Holland, Amsterdam, 1973), p. 221.

[9]B. Gabioud *et al.*, Phys. Lett. **103B**, 9 (1981).

[10]S. E. Vigdor *et al.*, in *Polarization Phenomena in Nuclear Physics—1980 (Fifth International Symposium, Sante Fe),* Proceedings of the Fifth International Symposium on Polarization Phenomena in Nuclear Physics, AIP Conf. Proc. No. 69, edited by G. G. Ohlson, R. E. Brown, N. Jarmie, M. W. McNaughton, and G. M. Hale (AIP, New York, 1981), p. 1455; L. D. Knutson *et al.*, Proceedings of the Charge Symmetry Breaking Workshop, Vancouver, 1981, TRIUMF Report TRI-81-3, 1981.

[11]W. T. H. van Oers, Bull. Am. Phys. Soc. **30**, 787 (1985); Nucl. Phys. **A416**, 267c (1984); L. G. Greeniaus, Proceedings of the Charge Symmetry Breaking Workshop, Vancouver, 1981, TRIUMF Report TRI-81-3, 1981.

[12]J. A. Nolen, Jr. and J. P. Schiffer, Annu. Rev. Nucl. Sci. **19**, 471 (1969).

[13]S. Shlomo, Rep. Prog. Phys. **41**, 957 (1978); N. Auerbach, V. Bernard, and N. van Giai, Phys. Rev. C **21**, 744 (1980).

[14]J. W. Negele, Nucl. Phys. **A165**, 305 (1971).

[15]J. W. Negele, in *Proceedings of the International Conference on Nuclear Structure and Spectroscopy,* edited by H. P. Blok and A. E. L. Dieperink (Scholars Press, Amsterdam, 1974).

[16]R. P. DeVito, S. M. Austin, W. Sterrenburg, and U. E. P. Berg, Phys. Rev. Lett. **47**, 628 (1981).

[17]G. A. Miller, private communication. Miller estimates an equivalent $J^{\rm CSB}$ from the hybrid quark-nucleon model no larger than about -10 MeV fm^3. This is smaller than the Negele value of -19 MeV fm^3 (Refs. 14 and 15) partly because the six-quark bag model does not quite account for all of the ^{41}Ca-^{41}Sc mass difference.

[18]R. K. Bhowmik, R. R. Doering, L. E. Young, S. M. Austin, A. Galonsky, and S. D. Schery, Nucl. Instrum. Methods **143**, 63 (1977); R. P. DeVito, Ph.D. thesis, Michigan State University, 1979; R. P. DeVito, S. M. Austin, U. E. P. Berg, W. Sterrenburg, and L. E. Young, Nucl. Instrum. Methods **215**, 423 (1983).

[19]We implicitly assume that the Coulomb part of the optical potential is local. An estimate based on the size of the exchange matrix element for the ground state of mass-41 (Refs. 12 and 14) of the change in the real nuclear potential caused by this assumption indicates it is less than $+0.3$ MeV. This corresponds to a change of about -5 MeV fm^3 in $J^{\rm CSB}$, which is small but not negligible.

[20]F. G. Perey, Phys. Rev. **131**, 745 (1963).

[21]R. De Leo, G. D'Erasmo, A. Pantaleo, G. Pasquariello, G. Viesti, M. Pignanelli, and H. V. Geramb, Phys. Rev. C **19**,

646 (1979).
[22]R. P. DeVito, S. M. Austin, U. E. P. Berg, R. DeLeo, and W. A. Sterrenburg, Phys. Rev. C **28**, 2530 (1983).
[23]R. de Swiniarski, H. E. Conzett, C. R. Lamontagne, B. Frois, and R. J. Slobodrian, Can. J. Phys. **51**, 1293 (1973).
[24]J. Raynal, computer code ECIS, CEN-Saclay, 1979.
[25]B. A. Brown, C. R. Bronk, and P. E. Hodgson, J. Phys. G **10**, 1683 (1984).
[26]R. Tailor, Ph.D. thesis, Ohio University, 1983.
[27]J. Rapaport, J. D. Carlson, D. Bainum, T. S. Cheema, and R. W. Finlay, Nucl. Phys. **A286**, 232 (1977).
[28]R. De Leo, G. D'Erasmo, E. Fabrici, S. Micheletti, A. Pantaleo, M. Pignanelli, and F. Resmini, Frascati National Laboratory Report INFN/BE-78/8, 1978.
[29]R. De Leo *et al.*, Nuovo Cimento **59A**, 101 (1980).
[30]G. Haouat, Ch. Lagrange, R. de Swiniarski, F. Dietrich, J. P. Delaroche, and Y. Pain, Phys. Rev. C **30**, 1795 (1984).
[31]R. De Leo, G. D'Erasmo, F. Ferrero, A. Pantaleo, and M. Pignanelli, Nucl. Phys. **A254**, 156 (1975).
[32]A. S. Meigooni, J. S. Petler, and R. W. Finlay, Phys. Med. Biol. **29**, 643 (1984); A. S. Meigooni, R. W. Finlay, J. S. Petler, and J. P. Delaroche, Nucl. Phys. A (in press).
[33]R. De Leo, G. D'Erasmo, A. Pantaleo, M. N. Harakeh, E. Cereda, S. Micheletti, and M. Pignanelli, Phys. Rev. C **28**, 1443 (1983).
[34]E. P. Lippincott and A. M. Bernstein, Phys. Rev. **163**, 1170 (1967).
[35]W. T. H. van Oers, Phys. Rev. C **3**, 1550 (1971).
[36]B. A. Brown, S. E. Massen, and P. E. Hodgson, J. Phys. G **5**, 1655 (1979).
[37]E. Auerbach, S. Kahana, and J. Weneser, Phys. Rev. Lett. **23**, 1253 (1969).
[38]B. A. Brown, private communication.
[39]N. van Giai and H. Sagawa, Phys. Lett. **106B**, 379 (1981).
[40]M. Beiner, H. Flocard, N. van Giai, and P. Quentin, Nucl. Phys. **A238**, 29 (1975).
[41]E. Fabrici, S. Micheletti, M. Pignanelli, F. G. Resmini, R. De Leo, G. D'Erasmo, A. Pantaleo, J. L. Escudie, and A. Tarrats, Phys. Rev. C **21**, 830 (1980).
[42]Y. R. Gaillard *et al.*, Nucl. Phys. **A327**, 349 (1979).
[43]J. Lowe and D. L. Watson, Phys. Lett. **23**, 261 (1966).
[44]D. J. Hughes and R. B. Schwartz, *Neutron Cross Sections*, 2nd ed. (U.S. GPO, Washington, D.C., 1958).
[45]D. I. Garber and R. R. King, *Neutron Cross Sections*, 3rd ed. (National Technical Information Service, U.S. Dept. of Commerce, Washington, D.C., 1976).
[46]J. Rapaport, Phys. Rep. **87**, 25 (1982).
[47]R. S. Mackintosh and A. M. Kobos, Phys. Lett. **62B**, 127 (1976).

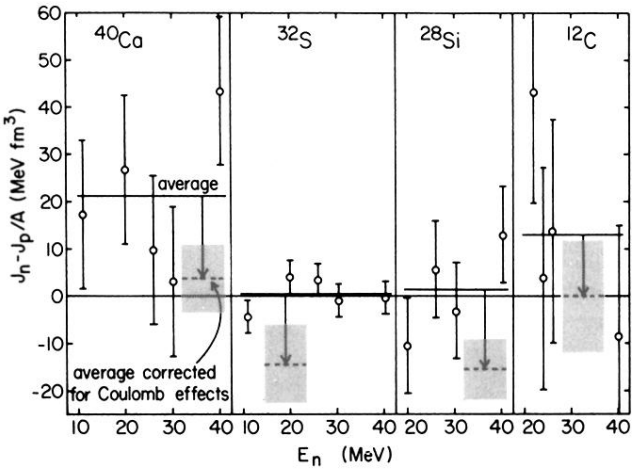

FIG. 5. Differences of the real volume integrals per nucleon for proton and neutron scattering from ^{40}Ca, ^{32}S, ^{28}Si, and ^{12}C. The points are the differences between the fitted line for protons (Figs. 4, 6, 7, and 9) and the measured values for neutrons. The solid lines are the averages of these differences in each case, the error bars on the points show the standard deviation about this mean. The dashed lines within the shaded regions are the averages with their associated uncertainties after correcting for Coulomb effects.